Geomechanics and Engineering, *Vol. 9, No. 4 (2015) 427-445*
DOI: http://dx.doi.org/10.12989/gae.2015.9.4.427

Surrounding rock pressure of shallow-buried bilateral bias tunnels under earthquake

Xin-Rong Liu [1,2], Dong-Liang Li [*1,2], Jun-Bao Wang [3] and Zhen Wang [1,2]

[1] *School of Civil Engineering, Chongqing University, Chongqing 400045, China*
[2] *Key Laboratory of New Technology for Construction of Cities in Mountain Area (Chongqing University), Ministry of Education, Chongqing 400045, China*
[3] *School of Civil Engineering, Xi'an University of Architecture and Technology, Xi'an, 710055, China*

(*Received April 04, 2015, Revised May 15, 2015, Accepted May 20, 2015*)

Abstract. By means of finite element numerical simulation and pseudo-static method, the shallow-buried bilateral bias twin-tube tunnel subject to horizontal and vertical seismic forces are researched. The research includes rupture angles, the failure mode of the tunnel and the distribution of surrounding rock relaxation pressure. And the analytical solution for surrounding rock relaxation pressure is derived. For such tunnels, their surrounding rock has sliding rupture planes that generally follow a "W" shape. The failure area is determined by the rupture angles. Research shows that for shallow-buried bilateral bias twin-tube tunnel under the action of seismic force, the load effect on the tunnel structure shall be studied based on the relaxation pressure induced by surrounding rock failure. The rupture angles between the left tube and the right tube are independent of the surface slope. For tunnels with surrounding rock of Grade IV, V and VI, which is of poor quality, the recommended reinforcement range for the rupture angles is provided when the seismic fortification intensity is VI, VII, VIII and IX respectively. This study is expected to provide theoretical support regarding the ground reinforcement range for the shallow-buried bilateral bias twin-tube tunnel under seismic force.

Keywords: pseudo-static method; earthquake force; bilateral bias; tunnel; rupture angle

1. Introduction

A bias tunnel is one that is under obviously asymmetric force. This special form of load makes its design and support clearly distinguished from common tunnels (Feldgun *et al*. 2014, Mollon *et al*. 2011, Simanjuntak *et al*. 2014, Kalitsov *et al*. 2013). According to the data on the collapse of 1025 tunnels, a representative calculation model of surrounding rock pressure was brought forward, in which the overlying rock mass of the tunnel under limit state was regarded as loose rock to establish a formula for the calculation of surrounding rock pressure on the unilateral bias tunnel (Prasad *et al*. 2013). This calculation model has become a common practice as it is safe in actual project design. The model is also used in design codes in China to calculate the lining load of the tunnel. In addition, Shao and Macari (2008) made a theoretical analysis of the unilateral bias neighborhood tunnel in order to calculate its surrounding rock pressure. Li *et al*. (2014) analyzed

∗Corresponding author, Ph.D. Student, E-mail: ylfy21@126.com

http://www.techno-press.org/?journal=gae&subpage=7 ISSN: 2005-307X (Print), 2092-6219 (Online)

the stability of the surrounding rock and stress characteristics of supporting structure of the shallow-buried bias tunnel based on the engineering projects as well as site monitoring and measurement data. Roateşi (2014) studied the excavation and construction plan of shallow-buried bias tunnels through finite element numerical simulation, and proposed a new construction plan that met the requirement for tunnel stability. There is no shortage of such researches on unilateral bias tunnels. However, little systematic research has been conducted on bilateral bias tunnels, which are more complicated because of topographical limitations (Saada *et al*. 2013, Scussel and Chandra 2014, Pinyol and Alonso 2012).

In recent years, earthquake disasters are growing in frequency (Bilotta *et al*. 2012, Kouretzis *et al*. 2013). People's demand for durability and safety of bias tunnels can no longer be satisfied merely through static analysis, and the seismic capacity of these tunnels is receiving growing concern (Sahoo and Kumar 2012, Gomes 2013). Sanchez-Merino *et al*. (2009) conducted researches on the simple longitudinal seismic response of tunnel linings subject to surface wave. Yang *et al*. (2010), with the effect of horizontal seismic load taken into consideration, analyzed the surrounding rock pressure on the shallow-buried unilateral bias tunnels. Furthermore, El Naggar *et al*. (2008) presents an analytical procedure for evaluating in-plane moments and thrusts in composite and jointed tunnel linings during earthquakes.

From relevant literature, it is known that previous researches on seismic solution of tunnels mainly focus on the effect of horizontal seismic force (Chakraborty and Kumar 2013, Senent *et al*. 2013, Milev *et al*. 2001, Hiroyasu *et al*. 2007). In practice, however, the earthquake acceleration is a variable of great uncertainty in direction (Debiasi *et al*. 2013). For example, a violent earthquake struck Wenchuan, China in 2008. Numerous buildings are damaged, in which the vertical seismic force also played a role, apart from the horizontal seismic force (Guo *et al*. 2014). Therefore, it is not enough to just focus on the horizontal seismic force.

In this paper, shallow-buried bilateral bias tunnels are studied on the basis of existing research methods while considering the combined effect of horizontal and vertical seismic forces. With the pseudo-static method, the analytical solution for shallow-buried bilateral bias tunnels under the action of seismic force is derived and used for analysis of the rupture angles at both sides of the tunnel.

2. Structural load and failure mode of the tunnel

Surrounding rock pressure is the main load on the tunnel structure. According to the geological conditions and the structural features of the tunnel, surrounding rock pressure consists of relaxation pressure and deformation pressure (Holter 2014). Shallow-buried bilateral bias tunnels are mainly distributed in steep mountain areas. Due to the poor geological conditions there, surrounding rock of the tunnel is easily weathered. In the event of an earthquake, the weathered rock will invoke relaxation pressure, to which special attention shall be paid. Therefore, the load on shallow-buried bilateral bias tunnels when an earthquake occurs shall be based on the relaxation pressure as a result of surrounding rock failure.

There are so far few studies regarding the effect of horizontal and vertical seismic force together on shallow-buried bilateral bias tunnels. However, the surrounding rock pressure calculation model for shallow-buried unilateral bias tunnels established by Zhong *et al*. (2013) makes a good reference. By means of field investigation and numerical analysis, Zhong *et al*. (2013) analyzed the failure mode of shallow-buried bilateral bias twin-tube tunnel: The left

sidewall of the left tube and the right sidewall of the right tube are where stress is most concentrated. The rupture surface starts from the sidewalls and expands out and upward at a certain dip angle until it reaches the slope surface. The rock-soil mass is assumed to be an isotropic homogeneous continuous medium. According to the failure mode, the surrounding rock was divided into several relatively independent parts to be analyzed. The research showed that the failure area of shallow-buried bilateral bias twin-tube tunnel was dependent on the rupture angles. And the horizontal lateral pressure coefficients (λ_A, λ_B, λ_C, λ_D) were derived as follows

$$\lambda_A = \frac{1}{\tan\beta_A + \tan\alpha_L} \cdot \frac{\tan\beta_A - \tan\varphi_c}{1 + \tan\beta_A\left(\tan\varphi_c - \tan\theta\right) + \tan\varphi_c \tan\theta} \tag{1}$$

$$\lambda_B = \frac{a_1(h_{L2} + H_t + h_0)}{h_{L2}^2} \cdot \frac{\tan\beta_B - \tan\varphi_c}{1 + \tan\beta_B\left(\tan\varphi_c - \tan\theta\right) + \tan\varphi_c \tan\theta} \tag{2}$$

$$\lambda_C = \frac{a_2(h_{R1} + H_t + h_0)}{h_{R1}^2} \cdot \frac{\tan\beta_C - \tan\varphi_c}{1 + \tan\beta_C\left(\tan\varphi_c - \tan\theta\right) + \tan\varphi_c \tan\theta} \tag{3}$$

$$\lambda_D = \frac{1}{\tan\beta_D + \tan\alpha_R} \cdot \frac{\tan\beta_D - \tan\varphi_c}{1 + \tan\beta_D\left(\tan\varphi_c - \tan\theta\right) + \tan\varphi_c \tan\theta} \tag{4}$$

Where β_A, β_B, β_C and β_D are rupture angles, φ_c is the calculated friction angle, θ is the internal friction angle and the other geometric parameters are as shown in Fig. 2.

In order to establish a calculation model for the structural load of shallow-buried bilateral bias tunnels subject to both horizontal and vertical seismic forces, the loose zone and failure mode of the surrounding rock under seismic force shall be clearly defined. Through field investigation and data collection regarding some of the existing shallow-buried bilateral bias tunnels, a numerical model is established using the finite element software ANSYS. In this model, Strength Reduction Finite Element Method is adopted to analyze the deformation and plastic zone distribution of surrounding rock in limit equilibrium state under the action of both horizontal and vertical seismic load.

To demonstrate its basic distribution pattern, the surrounding rock of tunnel is treated as a homogeneous body, without regard to the joint fissure and material change of the rock mass. As the tunnel is shallow-buried, the initial stress of the formation is the gravity stress, without regard to structural stress. The elasto-plastic constitutive model under the Drucker-Prager yield criterion is used. After excavation, the tunnel is immediately protected by the primary support. The research is conducted under the most unfavorable conditions, i.e., seismic load is applied without secondary lining after the excavation is completed.

The numerical analysis by applying seismic wave of intensities VI, VII, VIII and IX to tunnels with different surface slopes and surrounding rock grades shows that the expansion of plastic zone of surrounding rock follows a certain pattern. The outer sidewalls of the left and right tubes are where stress is most concentrated. Plastic failure starts from here and expands out and upward at a certain dip angle until it reaches the slope surface. Plastic zones also exist in the inner sidewall of left and right tubes. Similarly, they expand upward at a certain dip angle and intersect near the middle rock pillar. The whole plastic zone forms a successive shear plane in a shape of “W”, as shown in Fig. 1 (The seismic wave intensity corresponds to Fig .1 is VI and the input data of the

Table 1 The physical and mechanical parameters

	Volume weight γ (kN/m^3)	Elastic modulus E (GPa)	Poisson ratio μ	Cohesive c (MPa)	Internal friction angle θ (°)
Surrounding rock	20	1.5	0.35	0.12	22.4
Reinforcement ring	21	1.5	0.35	0.28	22.4
Primary support	25	27.7	0.2	-	-

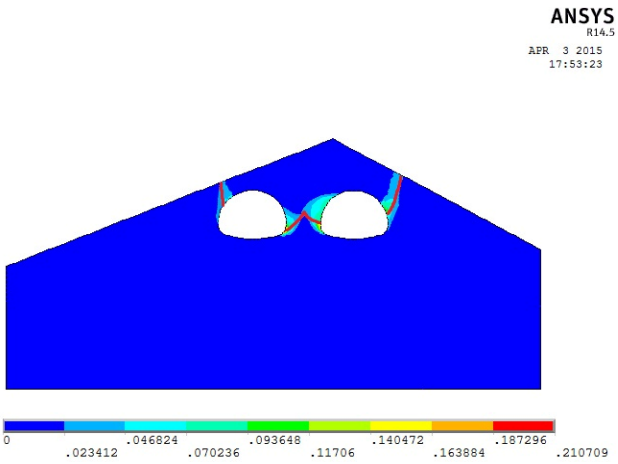

Fig. 1 The failure model of tunnel

model are shown in Table 1).

Meanwhile, it can be easily known that at the upper part of "W", the surrounding rock is loose and damaged, i.e., the rock mass is limited by the rupture angles of the tunnel. Here is the basic failure mode of surrounding rock for shallow-buried bilateral bias tunnels with both horizontal and vertical seismic forces taken into consideration. The area of damaged surrounding rock is determined by the rupture angles at both sides of the tunnel. Based on this failure mode, a calculation model for the structural load of shallow-buried bilateral bias tunnels when subject to seismic load is established to ensure tunnel stability in the event of an earthquake.

3. Calculation of structural load

3.1 Basic assumptions

The above analysis shows that the failure area of shallow-buried bilateral bias tunnels under seismic force is dependent on the rupture angles at both sides of the tunnel. This is consistent with the concept involved in the calculation model proposed by Zhong *et al*. (2013), indicating the model is reasonable and feasible. Considering the research results above and Fig. 2 together, the following assumption can be made:

(1) The rock-soil mass is an isotropic homogeneous continuous medium.
(2) Surface dip angle is α_L at the left side, and α_R at the right side of the tunnel. In the rock-soil

mass at the left side of the left tube, there forms sliding rupture plane AC. The angle between AC and the horizontal planes is the rupture angle β_1. In the rock-soil mass at the right side of the left tube, there forms sliding rupture plane GL. The angle between GL and the horizontal plane is the rupture angle β_2. In the rock-soil mass at the left side of the right tube, there forms sliding rupture plane NH. The angle between NH and the horizontal plane is the rupture angle β_3. Meanwhile, the sliding rupture plane GL intersects with NH at O near the middle rock pillar. As the tunnel is under unsymmetrical pressure, the point of intersection O deviates from the center line of the middle rock pillar at a certain distance (Fig. 2). In the rock-soil mass at the right side of the right tube, there forms sliding rupture plane PS. The angle between PS and the horizontal plane is the rupture angle β_4.

(3) For the quadrilateral HOLK, the motion of rock mass at both sides of the bias tunnel produces a tensile rupture plane in the vertical plane IO. As a result, the sliding rupture plane at the right side of the left tube changes to GOI, and that at the left side of the right tube changes to NOI.

(4) Given the mountain deformation and tunnel failure mode, assume the rock-soil mass (BDEF and JMRQ) at the vault of left and right tubes sink, driving the sinking of rock-soil mass (ABC/GOIF and NOIJ/PQS) from both sides. However, when the whole rock-soil mass starts to sink and slide, its downward movement is impeded by resistances (F_1, F_2, F_3 and F_4) from unaffected rock-soil mass.

(5) Sliding rupture planes AC, GOI, NOI and PS are hypothetical. Their shear strength is determined by the calculated friction angle φ. The other flat planes BC, FG, NG and PQ are not sliding rupture planes for real, but hypothetical to facilitate the analysis. Therefore, the resistance of sliding surface is smaller than that of a real rupture plane, and the internal friction angle (θ) of the sliding surface is smaller the calculated one (φ).

3.2 Calculation of surrounding rock pressure

According to the pseudo-static method (Nouria *et al*. 2008), the inertia force in the horizontal and vertical directions generated during an earthquake is as follows

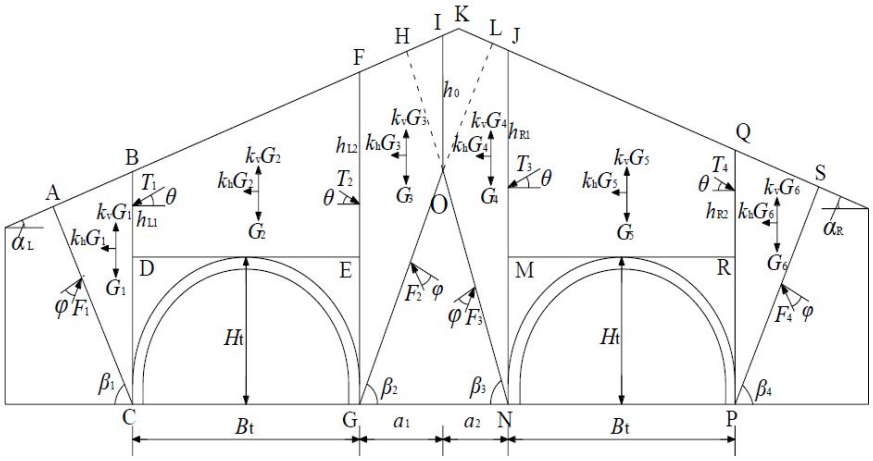

Fig. 2 Calculation model of shallow-buried bilateral bias twin-tube tunnel under earthquake force

$$\begin{cases} F_h = \dfrac{\alpha_h G}{g} = k_h G \\ F_v = \dfrac{\alpha_v G}{g} = k_v G \end{cases} \tag{5}$$

Where G is the weight of rock-soil mass and g is the acceleration of gravity. α_h and α_v is the pseudo static acceleration in the horizontal and vertical direction respectively. k_h is the pseudo static acceleration factor in the horizontal direction. When the seismic intensity is VI, VII, VIII and IX respectively, its value is 0.05, 0.10, 0.20 and 0.40. k_v is the pseudo static acceleration factor in the vertical direction. In gerenal, k_v = (1/2 ~ 2/3) k_h.

3.2.1 The left tube

(1) Lateral horizontal pressure at the left side

The left rock-soil mass ABC is selected for study. Its load and geometric parameters are shown in Fig. 3. γ (kN/m^3) is the volume weight of rock-soil mass and G_1 (kN/m) is the weight of ABC.

$$G_1 = \frac{1}{2}\gamma(h_{L1} + H_t)^2 \cdot \frac{1}{\tan\alpha_L + \tan\beta_1} \tag{6}$$

When an earthquake occurs, the rock-soil mass ABC is affected by seismic load. According to Eq. (5) and Eq. (6), inertia force will be generated in the horizontal (k_hG_1) and vertical (k_vG_1) directions of the rock-soil mass. See Fig. 4(a) for its force analysis. T_1 is the sliding force on plane BC generated when ABC, driven by the sinking of overlying rock-soil mass of the tunnel, slides.

On the basis of the pseudo-static method, the inertia forces k_hG_1 and k_vG_1 are regarded as dead load for composition with G_1. Their resultant force is G_1'. The angle between G_1' and the plumb line is η (°), as shown in Fig. 4(b). η is the seismic force deflection angle.

$$\eta = \arctan\frac{k_h}{1 - k_v} \tag{7}$$

It can be easily known that

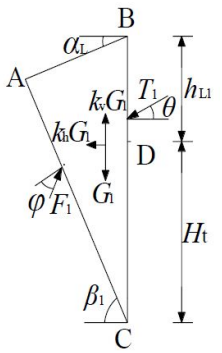

Fig. 3 Load of calculation diagram of rock mass ABC

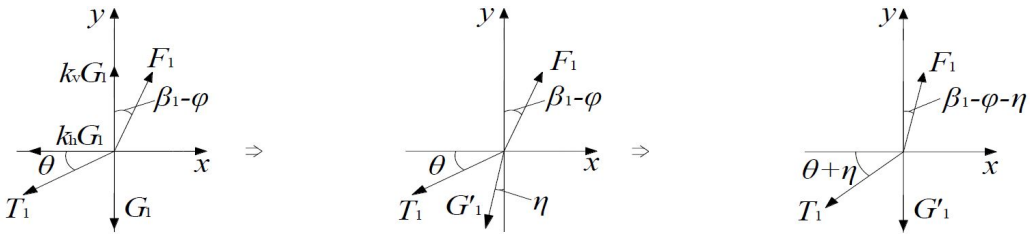

Fig. 4 Calculation diagram of rock mass ABC

$$G_1' = (1 - k_v)\ G_1 \sec\eta \tag{8}$$

In order for the resultant force G_1' to be in vertical direction so that calculation is easier, Fig. 4(b) is rotated η degrees counterclockwise, as shown in Fig. 4(c). The rotation does not change the equilibrium of force system and geometrical relationship between force, so the calculation results of lateral horizontal pressure will not be changed.

As shown in Fig. 4(c), from the equilibrium of forces we get

$$\begin{cases} F_1 \sin(\beta_1 - \varphi - \eta) = T_1 \cos(\theta + \eta) \\ F_1 \cos(\beta_1 - \varphi - \eta) = T_1 \sin(\theta + \eta) + G_1' \end{cases} \tag{9}$$

$$T_1 = \frac{G_1' \tan(\beta_1 - \varphi - \eta)}{\cos(\theta + \eta) - \sin(\theta + \eta)\tan(\beta_1 - \varphi - \eta)} \tag{10}$$

where

$$\tan(\beta_1 - \varphi - \eta) = \frac{\tan\beta_1 - \tan(\varphi + \eta)}{1 + \tan\beta_1 \tan(\varphi + \eta)} \tag{11}$$

By substituting Eqs. (6), (7) and (8) into Eq. (10), we get

$$T_1 = \frac{1}{2}\gamma(h_{L1} + H_t)^2 \frac{1 - k_v}{\cos(\theta+\eta)\cos\eta} \cdot \frac{1}{\tan\alpha_L + \tan\beta_1} \cdot \frac{\tan\beta_1 - \tan(\varphi+\eta)}{1 + \tan\beta_1\left[\tan(\varphi+\eta) - \tan(\theta+\eta)\right] + \tan(\varphi+\eta)\tan(\theta+\eta)} \tag{12}$$

Let the horizontal lateral pressure coefficient for the left side be λ_1, then

$$\lambda_1 = \frac{1 - k_v}{\cos\eta} \cdot \frac{1}{\tan\alpha_L + \tan\beta_1} \cdot \frac{\tan\beta_1 - \tan(\varphi+\eta)}{1 + \tan\beta_1\left[\tan(\varphi+\eta) - \tan(\theta+\eta)\right] + \tan(\varphi+\eta)\tan(\theta+\eta)} \tag{13}$$

Substitute Eq. (13) into Eq. (12) and we get

$$T_1 = \frac{1}{2}\gamma(h_{L1} + H_t)^2 \cdot \frac{\lambda_1}{\cos(\theta+\eta)} \tag{14}$$

According to Eq. (13), the lateral pressure coefficient λ_1 is determined by η, φ, θ and β_1, where θ can be determined by φ. In general, all values but rupture angle β_1 are known. Thus, the value of sliding force T_1 changes only with β_1. β_1 is a hypothetical rupture angle instead of a natural one in limit state. The real rupture angle is most likely to exist in the position where T_1 reaches its maximum.

Let $d\lambda_1/d\tan\beta_1 = 0$ and we get the tangent value of left rupture angle β_1 when T_1 reaches the maximum.

$$\tan\beta_1 = \tan(\varphi+\eta) + \sqrt{\frac{\left[\tan^2(\varphi+\eta)+1\right]\cdot\left[\tan\alpha_L + \tan(\varphi+\eta)\right]}{\tan(\varphi+\eta) - \tan(\theta+\eta)}} \tag{15}$$

Where φ is the calculated friction angle of plane AC, θ the friction angle of plane BC and $\theta < \varphi$. θ can be determined by φ. It is evident that β_1 can be determined by φ, η and α_L.

The horizontal lateral pressure is assumed to be linearly distribution in the vertical direction. The horizontal lateral pressure for the left side is

$$\begin{cases} e_1 = \gamma h_{L1}\lambda_1 \\ e_1' = \gamma(H_t + h_{L1})\ \lambda_1 \end{cases} \tag{16}$$

Where e_1 is the minimum horizontal lateral pressure and e_1' is the maximum horizontal lateral pressure.

(2) Lateral horizontal pressure at the right side

The left rock-soil mass GOIF is selected for study. T_2 is the sliding force on plane CE generated when GOIF, driven by the sinking of overlying rock mass of the tunnel, slides. The remaining loads are discussed above. See Fig. 5 for the loads and geometric parameters, and see Fig. 6 for force analysis.

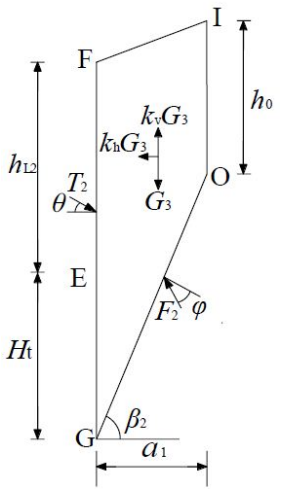

Fig. 5 Load of calculation diagram of rock mass GOIF

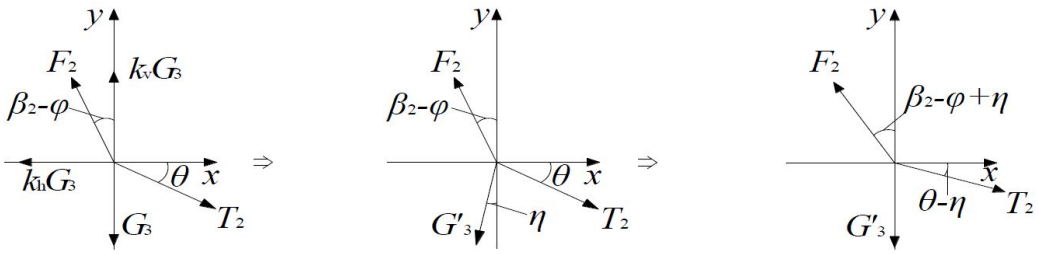

(a) (b) (c)

Fig. 6 Calculation diagram of rock mass GOIF

It can be easily known that

$$G_3 = \frac{1}{2}\gamma a_1 (H_t + h_{L2} + h_0) \tag{17}$$

$$G_3' = (1 - k_v)\ G_3 \sec\eta \tag{18}$$

$$T_2 = \frac{G_3' \tan(\beta_2 - \varphi + \eta)}{\cos(\theta - \eta) - \sin(\theta - \eta)\tan(\beta_2 - \varphi + \eta)} \tag{19}$$

$$T_2 = \frac{1}{2}\gamma a_1 (H_t + h_{L2} + h_0)\frac{1 - k_v}{\cos(\theta - \eta)\cos\eta} \cdot \frac{\tan\beta_2 - \tan(\varphi - \eta)}{1 + \tan\beta_2\left[\tan(\varphi - \eta) - \tan(\theta - \eta)\right] + \tan(\varphi - \eta)\tan(\theta - \eta)} \tag{20}$$

Let the horizontal lateral pressure coefficient for the right side be λ_2, then

$$\lambda_2 = \frac{a_1 (H_t + h_{L2} + h_0)}{h_{L2}^2} \cdot \frac{1 - k_v}{\cos\eta} \cdot \frac{\tan\beta_2 - \tan(\varphi - \eta)}{1 + \tan\beta_2\left[\tan(\varphi - \eta) - \tan(\theta - \eta)\right] + \tan(\varphi - \eta)\tan(\theta - \eta)} \tag{21}$$

$$T_2 = \frac{1}{2}\gamma h_{L2}^2 \cdot \frac{\lambda_2}{\cos(\theta - \eta)} \tag{22}$$

It is known from the geometrical relationship that $a_1 = m/\tan\beta_2$, where m is the distance from O to GN.

Similar to Section 3.2.1-(1), let $d\lambda_2/d\tan\beta_2 = 0$ so that T_2 reaches its maximum, and we get

$$\tan\beta_2 = \tan(\varphi - \eta) + \sqrt{\tan^2(\varphi - \eta) + \frac{\tan(\varphi - \eta)\left[\tan(\varphi - \eta)\cdot\tan(\theta - \eta) + 1\right]}{\tan(\varphi - \eta) - \tan(\theta - \eta)}} \tag{23}$$

Where φ is the calculated friction angle of plane GO, θ the friction angle of plane FG and $\theta < \varphi$. θ can be determined by φ. It is evident that β_2 can be determined by φ and η.

The horizontal lateral pressure for the right side is

$$\begin{cases} e_2 = \gamma h_{L2}\lambda_2 \\ e_2' = \gamma(H_t + h_{L2})\ \lambda_2 \end{cases} \tag{24}$$

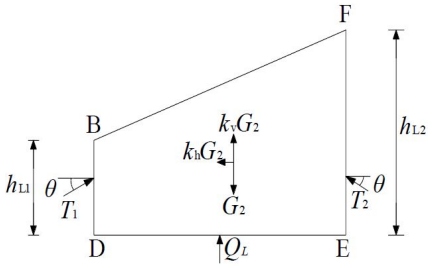

Fig. 7 Load of calculation diagram of rock mass BDEF under earthquake force

(3) Vertical pressure of surrounding rock at left tube vault

BD and FE are smaller than BC and FG, and the friction angle between the lining and soil are varies. BDEF is selected as the overlying rock-soil mass of the tunnel vault. For the rock-soil mass BDEF, G_2 is its weight, and T_1 and T_2 are same as above. Q_L is the overall counterforce of the left tube vault on BDEF. Its value equals the overall vertical pressure of BDEF on the vault. Parameters of BDEF under the action of horizontal and vertical seismic force are shown in Fig. 7.

It can be easily known that

$$G_2 = 0.5\gamma B_t(h_{L1} + h_{L2}) \tag{25}$$

As $\Sigma Y = 0$, it is obtained that

$$Q_L = (1 - k_v)\ G_2 - T_1 \sin\theta - T_2 \sin\theta \tag{26}$$

By substituting Eqs. (14), (22) and (25) into Eq. (26), we get

$$Q_L = \frac{1}{2}\gamma\left[B_t(1 - k_v)\cdot(h_{L1} + h_{L2}) - \frac{\lambda_1 h_{L1}^2}{\cos(\theta + \eta)} - \frac{\lambda_2 h_{L2}^2}{\cos(\theta - \eta)}\right] \tag{27}$$

Assume the distribution of bias pressure follows the same pattern with the surface slope, and Q_L can be converted into the uniform load on the supporting structure of left tube vault

$$q_L = \frac{1}{2}\gamma\left[(1 - k_v)\cdot(h_{L1} + h_{L2}) - \frac{\lambda_1 h_{L1}^2}{B_t\cos(\theta + \eta)} - \frac{\lambda_2 h_{L2}^2}{B_t\cos(\theta - \eta)}\right] \tag{28}$$

Let the vertical pressure of BDEF on side BD of top of left tube be q_1, and that on side FE be q_2. The rock-soil mass pressure changes in a linear fashion. So

$$\begin{cases} q_1 = q_L - \dfrac{B_t}{2}\tan\alpha_L \\ q_2 = q_L + \dfrac{B_t}{2}\tan\alpha_L \end{cases} \tag{29}$$

3.2.2 The right tube

For the right tube, the analysis procedure is similar to that of the left tube. Therefore, the following can be obtained.

(1) Lateral horizontal pressure at the left side

The weight of rock-soil mass IONJK can be approximately represented by the following equation

$$G_4 = \frac{1}{2}\gamma a_2(H_t + h_{R1} + h_0) \tag{30}$$

$$T_3 = \frac{1}{2}\gamma h_{R1}^2 \cdot \frac{\lambda_3}{\cos(\theta+\eta)} \tag{31}$$

The horizontal lateral pressure coefficient for the left side (λ_3)

$$\lambda_3 = \frac{a_2(H_t + h_{R1} + h_0)}{h_{R1}^2} \cdot \frac{1-k_v}{\cos\eta} \cdot \frac{\tan\beta_3 - \tan(\varphi+\eta)}{1+\tan\beta_3\left[\tan(\varphi+\eta) - \tan(\theta+\eta)\right] + \tan(\varphi+\eta)\tan(\theta+\eta)} \tag{32}$$

Where $a_2 = m/\tan\beta_3$ and m is the distance from O to GN.

Tangent value of rupture angle β_3

$$\tan\beta_3 = \tan(\varphi+\eta) + \sqrt{\tan^2(\varphi+\eta) + \frac{\tan(\varphi+\eta)\left[\tan(\varphi+\eta)\cdot\tan(\theta+\eta)+1\right]}{\tan(\varphi+\eta) - \tan(\theta+\eta)}} \tag{33}$$

The horizontal lateral pressure at the left side is

$$\begin{cases} e_3 = \gamma h_{R1}\lambda_3 \\ e_3' = \gamma(H_t + h_{R1})\ \ \lambda_3 \end{cases} \tag{34}$$

(2) Lateral horizontal pressure at the right side

$$T_4 = \frac{1}{2}\gamma(H_t + h_{R2})^2 \cdot \frac{\lambda_4}{\cos(\theta-\eta)} \tag{35}$$

The horizontal lateral pressure coefficient for the left side (λ_4)

$$\lambda_4 = \frac{1-k_v}{\cos\eta} \cdot \frac{1}{\tan\alpha_R + \tan\beta_4} \cdot \frac{\tan\beta_4 - \tan(\varphi-\eta)}{1+\tan\beta_4\left[\tan(\varphi-\eta) - \tan(\theta-\eta)\right] + \tan(\varphi-\eta)\tan(\theta-\eta)} \tag{36}$$

Tangent value of rupture angle β_4

$$\tan\beta_4 = \tan(\varphi-\eta) + \sqrt{\frac{\left[\tan^2(\varphi-\eta)+1\right]\cdot\left[\tan\alpha_R + \tan(\varphi-\eta)\right]}{\tan(\varphi-\eta) - \tan(\theta-\eta)}} \tag{37}$$

The horizontal lateral pressure at the right side is

$$\begin{cases} e_4 = \gamma h_{R2}\lambda_4 \\ e_4' = \gamma(H_t + h_{R2})\ \ \lambda_4 \end{cases} \tag{38}$$

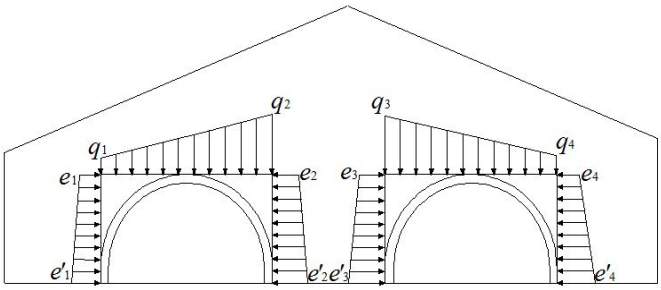

Fig. 8 Surrounding rock pressure distribution of shallow-buried bilateral bias tunnel under earthquake force

(3) Vertical pressure on surrounding rock at right tube vault

Assume the distribution of bias pressure follows the same pattern with the surface slope. The uniform load on the supporting structure of right tube vault is

$$q_R = \frac{1}{2}\gamma\left[(1-k_v)\cdot(h_{R1}+h_{R2}) - \frac{\lambda_3 h_{R1}^2}{B_t\cos(\theta+\eta)} - \frac{\lambda_4 h_{R2}^2}{B_t\cos(\theta-\eta)}\right] \tag{39}$$

Let the vertical pressure of JMRQ on side JM of top of left tube be q_3, and that on side QR be q_4. The rock-soil mass pressure changes in a linear fashion. So

$$\begin{cases} q_3 = q_R - \dfrac{B_t}{2}\tan\alpha_R \\ q_4 = q_R + \dfrac{B_t}{2}\tan\alpha_R \end{cases} \tag{40}$$

In light of the theoretical derivation above, the distribution of surrounding rock pressure for shallow-buried bilateral bias twin-tube tunnel subject to both horizontal and vertical seismic forces is shown in Fig. 8.

4. Comparison and verification

The calculation model for the structural load of shallow-buried bilateral bias tunnels when subject to horizontal and vertical seismic forces is a simplified model established to facilitate the seismic design of such tunnels. The calculation formulas obtained from theoretical derivation require further validation.

If the seismic load is not considered, the seismic force deflection angle $\eta = 0$. Then Eq. (13) and Eq. (37) can be simplified as

$$\lambda_1 = \frac{1}{\tan\alpha_L + \tan\beta_1}\cdot\frac{\tan\beta_1 - \tan\varphi}{1+\tan\beta_1(\tan\varphi - \tan\theta)+\tan\varphi\tan\theta} \tag{41}$$

$$\lambda_4 = \frac{1}{\tan\alpha_R + \tan\beta_4}\cdot\frac{\tan\beta_4 - \tan\varphi}{1+\tan\beta_4(\tan\varphi - \tan\theta)+\tan\varphi\tan\theta} \tag{42}$$

Eq. (21) and Eq. (32) can be simplified as

$$\lambda_2 = \frac{a_1(H_t + h_{L2} + h_0)}{h_{L2}^2} \cdot \frac{\tan\beta_2 - \tan\varphi}{1 + \tan\beta_2(\tan\varphi - \tan\theta) + \tan\varphi\tan\theta} \tag{43}$$

$$\lambda_3 = \frac{a_2(H_t + h_{R1} + h_0)}{h_{R1}^2} \cdot \frac{\tan\beta_3 - \tan\varphi}{1 + \tan\beta_3(\tan\varphi - \tan\theta) + \tan\varphi\tan\theta} \tag{44}$$

Through comparative analysis, Eqs. (41), (42), (43) and (44) are in full agreement with Eqs. (1), (4), (2) and (3) derived by Zhong *et al*. (2013). Thus it can be seen that the calculation model of surrounding rock relaxation pressure for shallow-buried bilateral bias tunnels established and analyzed by Zhong *et al*. (2013) is nothing but a special case – when the seismic load is 0 – involved in the model used in this paper. Therefore, the analysis ideas in this paper make sense, and the calculation model for the structural load of shallow-buried bilateral bias tunnels when subject to both horizontal and vertical seismic forces is reasonable.

5. Engineering case

5.1 Project overview

Zuanqianmen Tunnel is located in G1 section of Xinzhou-Debao Highway, Shanxi Province, China. It has four lanes in two directions and is a typical bilateral bias tunnel. The left tube is 271 m long and the right 265 m long, as shown in Fig. 9. In the shallow-buried bias section, the main rock mass is strongly weathered gneiss, with a surrounding rock grade of V and volume weight of 20 kN/m^3. Cross section A is selected for analysis. The left tube depth is 20.50 m, the right 16.24 m and the clear distance between them 13.2 m. Each tube is 12.56 m in width and 8.84 m in height. Surface dip angle α_L is 32°, and α_R is 25°.

5.2 Field monitoring of surrounding rock pressure

In order to monitor the surrounding rock pressure, a group of monitoring points is arranged in cross section A. See Fig. 10 for arrangement of the monitoring points and see Fig. 11 for the monitoring instrument.

Fig. 9 Zuanqianmen Tunnel

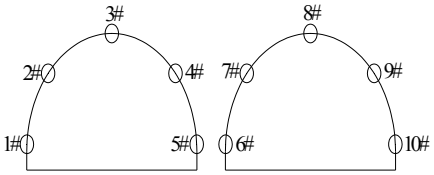

Fig. 10 The arrangement of the monitoring points

Fig. 11 The monitoring instrument

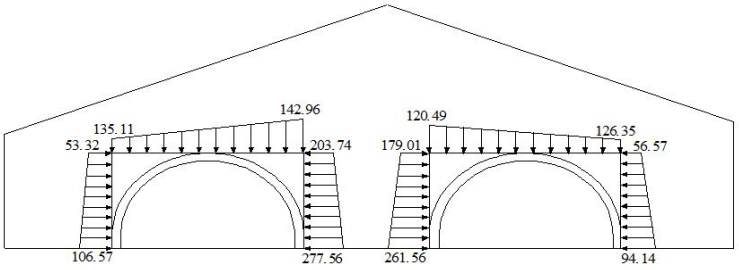

Fig. 12 Theoretical calculated values of surrounding rock pressure (kPa)

Table 2 The values of field monitoring and theoretical calculation (kPa)

Monitoring point	1#	2#	3#	4#	5#	6#	7#	8#	9#	10#
Theoretical calculated value	95.43	148.53	139.04	255.72	268.61	253.22	220.28	123.42	142.48	82.79
Field monitoring value	71.72	100.47	93.22	165.88	172.54	220.34	135.36	105.29	102.21	59.43

5.3 Comparison and analysis of field monitoring and theoretical calculation

The vertical and lateral horizontal surrounding rock pressure values can be determined by formulas (16), (24), (29), (34), (38) and (40) (See Fig. 12).

During the excavation, the region where the tunnel belongs was hit by a VI-magnitude earthquake. The surrounding rock pressure gauge detected the pressure change during the earthquake. For ease of comparison between theoretical values and field monitoring values, the vertical and lateral horizontal surrounding rock pressures are subject to vector composition and their resultant vector is applied to the tunnel. The theoretical and field monitoring values of each monitoring point are organized and shown in Table 2.

According to Table 2, it is found that the monitoring values of each point are smaller than theoretical ones. Behind this there are two reasons. First, the field monitoring instruments were installed after the excavation, when part of the surrounding rock pressure had been released and the released amount was not measurable. Second, the theoretical calculation is based on a series of assumptions and the limit equilibrium theory, while in actual it is impossible for the surrounding rock deformation to fully develop and even come into failure. According to the analysis of the

Table 3 Surrounding rock's parameters

Grade of surrounding rock	I	II	III	IV	V	VI
φ (°)	78.0	74.0	65.0	55.0	45.0	37.0
θ (°)	70.2	66.6	58.5	44.0	27.0	14.8

Table 4 The classification of surrounding rock

Surrounding rock	Volume weight γ (kN/m^3)	Elastic modulus E (GPa)	Poisson ratio μ	Cohesive c (MPa)
I	26-28	> 33	< 0.2	> 2.1
II	25-27	20-33	0.2-0.25	1.5-2.1
III	23-25	6-20	0.25-0.3	0.7-1.5
IV	20-23	1.3-6	0.3-0.35	0.2-0.7
V	17-20	1-2	0.35-0.45	0.05-0.2
VI	15-17	< 1	0.4-0.5	< 0.2

pressure values and value distribution of each monitoring point, the monitoring values are smaller than theoretical ones and they are similar to each other in distribution. Therefore, the use of this theoretical model to calculate surrounding rock pressure of the tunnel under the action of seismic load is safe and feasible. The rationality of the model established in Section 3 is verified as well.

6. Research on reinforcement range for rupture angle

According to the analysis of Yang *et al*. (2010) and Shagapov *et al*. (2002), different surrounding rock conditions are selected, as shown in Table 3. The classification of surrounding rock is shown in Table 4.

From Eq. (23) and Eq. (33), it is learnt that the rupture angles (β_2 and β_3) between the inside of left and right shallow-buried bilateral bias tunnels, when subject to both horizontal and vertical seismic forces, are not affected by the topography (independent of the surface slope).

When the seismic intensity is VI, VII, VIII and IX respectively, the coefficient of horizontal seismic acceleration k_h is 0.05, 0.10, 0.20 and 0.40. According to Eq. (7), it can be obtained that the seismic force deflection angle η is 3.0°, 6.1°, 13.0° and 28.7° respectively. According to Eq. (23), Eq. (33) and Table 3, the rupture angles β_2 and β_3 (Table 5) can be obtained when the twin-tube tunnel is under different surrounding rock conditions and seismic fortification intensities. A small amount of data is not listed because it is meaningless and the situation it represents is extremely rare in actual projects.

It is known from Table 5 that for the same grade of surrounding rock, the values of rupture angles β_2 and β_3 decrease with the increase of seismic intensity; for the same seismic intensity, the values of rupture angles β_2 and β_3 increase with the decrease of surrounding rock grade. When the seismic intensity is the same, for surrounding rocks of Grade I, II and III, each rise in grade leads to a slight 1°-2° decrease in β_2 and β_3; for poorer surrounding rocks of Grade IV, V and VI, each rise in grade causes much bigger decrease in β_2 (4.7° at least and 14.8° at most) and β_3 (3.4° at least and 5.4° at most). Therefore, under the same seismic intensity conditions, the values of β_2 and

Table 5 The calculated values of rupture angle β_2 and β_3

Seismic intensity	VI	VII	VIII	IX	VI	VII	VIII	IX
Grade of surrounding rock	β_2 (°)				β_3 (°)			
I	84.4	83.4	81.4	76.9	86.3	87.5	-	-
II	83.3	82.4	80.5	75.9	85.1	86.1	88.6	-
III	81.1	80.2	78.4	73.5	82.6	83.5	85.5	-
IV	76.4	75.4	72.8	65.2	78.4	79.4	81.7	87.2
V	70.3	68.8	65.0	52.1	73.0	74.3	77.0	83.0
VI	64.8	62.8	57.7	37.3	68.2	69.8	73.0	79.6

Table 6 The recommended reinforcement range for β_2 and β_3

Rupture angle	Seismic intensity			
	VI	VII	VIII	IX
β_2 (°)	62-79	60-78	55-75	35-68
β_3 (°)	66-81	67-82	71-84	77-90

β_3 for tunnels with poor surrounding rocks are more sensitive than those for tunnels with better surrounding rocks. They change in a much wider range and thus require additional attention.

To sum up, if the surrounding rock of the tunnel is of poor quality (Grade IV, V or VI), for safety purposes, a safety space of 2° is reserved for reinforcement, according to Table 5. See Table 6 for the recommended reinforcement range for β_2 and β_3.

For shallow-buried bilateral bias tunnel with poor surrounding rock (Grade IV, V or VI), values of β_1 and β_4 under different seismic fortification intensities when the surface slope changes from 15°-60° can be obtained from Eq. (15), Eq. (37) and Table 3. See Tables 7, 8 and 9.

Data in Table 7 show that surface slope has a significant influence on the values of β_1 and β_4. The larger the surface slope, the greater the values of β_1 and β_4. As an example, for shallow-buried bilateral bias tunnel with surrounding rock of grade IV, when the seismic fortification intensity is VI and the surface slope increases from 15° to 30°, 45° and 60°, the value of β_1 is 73.1°, 76.6°, 78.4° and 80.4° respectively, and the value of β_4 is 62.0°, 66.8°, 70.3° and 73.6° respectively. The same change rules can also be found from Table 8 and Table 9.

The values and variation trend listed in Table 7 reveal that when the surface slope is 15°-60°, for shallow-buried bilateral bias tunnels with surrounding rock of grade VI: if the seismic

Table 7 The calculated values of rupture angle β_1 and β_4 (Grade IV)

Seismic intensity	VI	VII	VIII	IX	VI	VII	VIII	IX
Surface slope	β_1 (°)				β_4 (°)			
15°	73.1	74.7	78.0	86.2	62.0	59.9	54.7	38.9
30°	76.3	77.5	80.2	86.8	66.8	65.1	60.7	46.3
45°	78.4	79.4	81.7	87.2	70.3	68.8	65.0	52.1
60°	80.4	81.2	83.0	87.6	73.6	72.3	69.2	58.0

Table 8 The calculated values of rupture angle β_1 and β_4 (Grade V)

Seismic intensity	VI	VII	VIII	IX	VI	VII	VIII	IX
Surface slope	β_1 (°)				β_4 (°)			
15°	65.8	67.7	71.7	80.3	70.1	68.5	64.6	53.6
30°	70.0	71.5	74.8	81.9	73.9	72.6	69.5	60.4
45°	73.0	74.3	77.0	83.0	76.4	75.4	72.8	65.2
60°	75.8	76.9	79.1	84.1	78.8	77.9	75.9	69.6

Table 9 The calculated values of rupture angle β_1 and β_4 (Grade VI)

Seismic intensity	VI	VII	VIII	IX	VI	VII	VIII	IX
Surface slope	β_1 (°)				β_4 (°)			
15°	59.5	61.7	66.2	75.5	55.0	52.4	45.9	24.9
30°	64.6	66.4	70.2	77.9	60.6	58.4	52.6	31.5
45°	68.2	69.8	73.0	79.6	64.8	62.8	57.7	37.3
60°	71.7	73.0	75.7	81.2	68.9	67.2	62.7	43.7

Table 10 The recommended reinforcement range for β_1 and β_4

Grade of surrounding rock	Rupture angle	Seismic intensity			
		VI	VII	VIII	IX
IV	β_1 (°)	71-83	72-84	76-85	84-90
	β_4 (°)	60-76	57-75	52-72	36-60
V	β_1 (°)	63-78	65-79	69-82	78-87
	β_4 (°)	68-81	66-80	62-78	51-72
VI	β_1 (°)	57-74	59-75	64-78	73-84
	β_4 (°)	53-71	50-70	43-65	22-46

fortification intensity is VI, the value of β_1 ranges from 73.1° to 80.4° and that of β_4 ranges from 62.0° to 73.6°; if the seismic fortification intensity is VII, the value of β_1 ranges from 74.7° to 81.2° and that of β_4 ranges from 59.9° to 72.3°; if the seismic fortification intensity is VIII, the value of β_1 ranges from 78.0° to 83.0° and that of β_4 ranges from 54.7° to 69.2°; if the seismic fortification intensity is IX, the value of β_1 ranges from 86.2° to 87.6° and that of β_4 ranges from 38.9° to 58.0°. Given the analysis above, a safety space of 2° is reserved for reinforcement as well. This helps get the recommended reinforcement range for β_1 and β_4 of shallow-buried bilateral bias tunnels with surrounding rock of Grade IV (and Grade V and VI, similarly) under different seismic fortification intensities. See Table 10.

7. Conclusions

- For shallow-buried bilateral bias tunnel located in rugged mountain areas, under the action of both horizontal and vertical seismic load, the load effect on the tunnel structure shall be

examined on the basis of the relaxation pressure induced by surrounding rock failure. And the surrounding rock mass under limit state shall be regarded as loose rock.

- Under the combined effect of horizontal and vertical seismic force, the basic failure mode for surrounding rock of shallow-buried bilateral bias twin-tube tunnel is: rupture planes develop in the outer sidewalls of left and right tubes and extend to the slope surface; sliding rupture planes develop in the sidewalls between left and right tubes, extend obliquely upward and intersect near the middle rock pillar. The whole rupture planes follows the shape of "W". The area of surrounding rock failure is determined by the values of the rupture angles at both sides of the tunnel.
- The calculation formulas for surrounding rock pressure and rupture angles in this failure mode are derived. Values of the rupture angles β_2 and β_3 between the left and right tubes are not affected by the topography (independent of the surface slope). For the same grade of surrounding rock, the greater the seismic intensity, the smaller the values of β_2 and β_3; for the same seismic intensity, the lower the grade of surrounding rock, the greater the values of β_2 and β_3.
- By studying the rupture angles β_1, β_2, β_3 and β_4 for tunnels with poor surrounding rock (Grade IV, V and VI), the recommended reinforcement ranges are given, which is expected to provide theoretical support regarding the ground reinforcement range for shallow-buried bilateral bias tunnels under the action of earthquakes.

Acknowledgments

The research described in this paper was financially supported by 2015 Chongqing graduate research and innovation project and the National Natural Science Foundation of China (41372356, 50334060). The financial supports are gratefully acknowledged by the authors!

References

Bilotta, E., Lanzano, G., Madabhushi, S.P.G. and Silvestri, F. (2014), "A numerical Round Robin on tunnels under seismic actions", *Acta Geotechnica*, **9**(4), 563-579.

Chakraborty, D. and Kumar, J. (2013), "Stability of a long unsupported circular tunnel in soils with seismic forces", *Nat. Hazard.*, **68**(2), 419-431.

Debiasi, E., Gajo, A. and Zonta, D. (2013), "On the seismic response of shallow-buried rectangular structures", *Tunn. Undergr. Space Technol.*, **38**, 99-113.

El Naggar, H., Hinchberger, S.D. and El Naggar, M.H. (2008), "Simplified analysis of seismic in-plane stresses in composite and jointed tunnel linings", *Soil Dyn. Earthq. Eng.*, **28**(12), 1063-1077.

Feldgun, V.R., Karinski, Y.S. and Yankelevsky, D.Z. (2014), "The effect of an explosion in a tunnel on a neighboring buried structure", *Tunn. Undergr. Space Technol.*, **44**, 42-45.

Gomes, R.C. (2013), "Effect of stress disturbance induced by construction on the seismic response of shallow bored tunnels", *Comput. Geotech.*, **49**, 338-351.

Guo, D.P., Hamada, M., He, C., Wang, Y.F. and Zou, Y.L. (2014), "An empirical model for landslide travel distance prediction in Wenchuan earthquake area", *Landslides*, **11**(2), 281-291.

Hiroyasu, O., Kazuo, S. and Nobusuke, H. (2007), "A study on the methodology of estimating the rock classification with the seismic exploration in mountain tunnel construction projects", *Zairyo/J. Soc. Mater. Sci., Japan*, **56**(9), 820-827. [In Japanese]

Holter, K.G. (2014) "Loads on sprayed waterproof tunnel linings in jointed hard rock: A study based on Norwegian cases", *Rock Mech. Rock Eng.*, **47**(3), 1003-1020.

Kalitsov, A., Zermatten, P.J., Bonell, F., Gaudin, G., Andrieu, S., Tiusan, C., Chshiev, M. and Velev, J.P. (2013), "Bias dependence of tunneling magnetoresistance in magnetic tunnel junctions with asymmetric barriers", *J. Phys.*: *Condensed Matter*, **25**(49), 1-8.

Kouretzis, G.P., Sloan, S.W. and Carter, J.P. (2013), "Effect of interface friction on tunnel liner internal forces due to seismic S- and P- wave propagation", *Soil Dyn. Earthq. Eng.*, **46**, 51-55.

Li, D.L., Liu, X.R. and Liu, F.M. (2014), "Analysis on stability of shallow buried and bias tunnel with different slope in loess", *Electron. J. Geotech. Eng.*, **19**, 6577-6588.

Milev, A.M., Spottiswoode, S.M., Rorke, A.J. and Finnie, G.J. (2001), "Seismic monitoring of a simulated rockburst on a wall of an underground tunnel", *J. South Af. Inst. Mining Metallur.*, **101**(5), 253-260.

Mollon, G., Dias, D. and Soubra, A.H. (2011), "Probabilistic analysis of pressurized tunnels against face stability using collocationbased stochastic response surface method", *J. Geotech. Geoenviron. Eng.*, *ASCE*, **137**(4), 385-397.

Nouria, H., Fakhera, A. and Jones, C.J.F.P. (2008), "Evaluating the effects of the magnitude and amplification of pseudo-static acceleration on reinforced soil slopes and walls using the limit equilibrium Horizontal Slices Method", *Geotext. Geomembr.*, **26**(3), 263-278.

Prasad, V.V.R., Dwivedi, R.D. and Swarup, A. (2013), "Determination of support pressure for tunnels and caverns using block theory", *Tunn. Undergr. Space Technol.*, **37**, 55-61.

Pinyol, N.M. and Alonso, E.E. (2012), "Design of micropiles for tunnel face reinforcement: undrained upper bound solution", *J. Geotech. Geoenviron. Eng.*, **138**(1), 89-99.

Roateşi, S. (2014), "Analytical and numerical approach for tunnel face advance in a viscoplastic rock mass", *Int. J. Rock Mech. Mining Sci.*, **70**, 123-132.

Saada, Z., Maghous, S. and Garnier, D. (2013), "Pseudo-static analysis of tunnel face stability using the generalized Hoek–Brown strength criterion", *Int. J. Numer. Anal. Method. Geomech.*, **37**(18), 3194-3212.

Sahoo, J.P. and Kumar, J. (2012), "Seismic stability of a long unsupported circular tunnel", *Comput. Geotech.*, **44**, 109-115.

Sanchez-Merino, A.L., Fernandez-Saez, J. and Navarro, C. (2009), "Simplified longitudinal seismic response of tunnels linings subjected to surface waves", *Soil Dyn. Earthq. Eng.*, **29**(3), 579-582.

Scussel, D. and Chandra, S. (2014), "New approach to the design of tunnels in squeezing ground", *Int. J. Geomech.*, **14**(1), 110-117.

Senent, S., Mollon, G. and Jimenez, R. (2013), "Tunnel face stability in heavily fractured rock masses that follow the Hoek-Brown failure criterion", *Int. J. Rock Mech. Mining Sci.*, **60**, 440-451.

Shagapov, V.S., Khusainova, G.Y., Khusainov, I.G. and Khazov, R.N. (2002), "Pressure relaxation in a hole surrounded by a porous and permeable rock", *Combust. Explo. Shock Waves*, **38**(3), 346-351.

Shao, Y. and Macari, E.J. (2008), "Information feedback analysis in deep excavations", *Int. J. Geomech.*, **8**(1), 91-103.

Simanjuntak, T.D.Y.F., Marence, M., Mynett, A.E. and Schleiss, A.J. (2014), "Pressure tunnels in non-uniform in situ stress conditions", *Tunn. Undergr. Space Technol.*, **42**, 227-236.

Yang, X.L., Huang, B. and Wang, Z.W. (2010), "Rock failure pressure of shallow tunnel subjected to horizontal seismic and unsymmetrical loads", *J. Central South Univ.* (*Science and Technology*), **41**(3), 1090-1095. [In Chinese]

Zhong, Z.L., Tu, Y.L., Liu, X.Y., Liu, Y.X. and Zhang, J. (2013), "Calculation of lining load of shallow-buried bilateral bias twin tunnel and its parameter sensitivity analysis", *China Civil Eng. J.*, **46**(1), 119-125. [In Chinese]

CC